Nanoscale

Accepted Manuscript

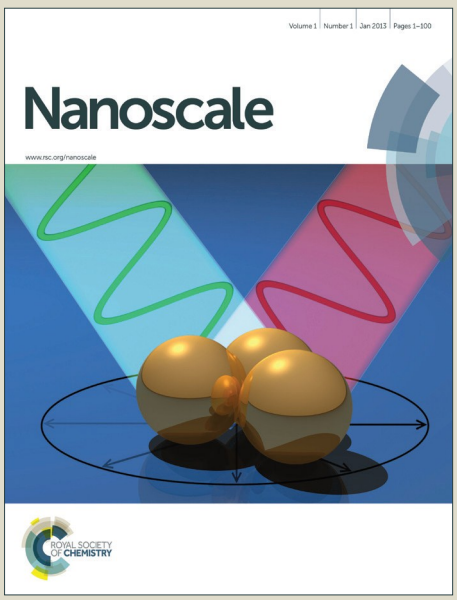

This is an *Accepted Manuscript*, which has been through the Royal Society of Chemistry peer review process and has been accepted for publication.

Accepted Manuscripts are published online shortly after acceptance, before technical editing, formatting and proof reading. Using this free service, authors can make their results available to the community, in citable form, before we publish the edited article. We will replace this *Accepted Manuscript* with the edited and formatted *Advance Article* as soon as it is available.

You can find more information about *Accepted Manuscripts* in the Information for Authors.

Please note that technical editing may introduce minor changes to the text and/or graphics, which may alter content. The journal's standard Terms & Conditions and the Ethical guidelines still apply. In no event shall the Royal Society of Chemistry be held responsible for any errors or omissions in this *Accepted Manuscript* or any consequences arising from the use of any information it contains.

ROYAL SOCIETY OF CHEMISTRY

www.rsc.org/nanoscale

Please do not adjust margins

Journal Name

ARTICLE

Self-supported Nanoporous $NiCo_2O_4$ Nanowires with Cobalt-nickel Layered Oxide Nanosheets for Overall Water Splitting

Received 00th January 20xx,
Accepted 00th January 20xx

DOI: 10.1039/x0xx00000x

www.rsc.org/

Jie Yin,[a] Panpan Zhou,[a] Li An,[a] Liang Huang,[a] Changwei Shao,[c] Jun Wang,[c] Hongyan Liu[a] and Pinxian Xi*[a,b]

Water splitting via the hydrogen evolution reaction (HER) and oxygen evolution reaction (OER) in producing H_2 and O_2 is a very important process in the energy field. Developing an efficient catalyst which can be applied into both HER and OER is crucial. Here, a bifunctional catalyst, CFP/$NiCo_2O_4$/$Co_{0.57}Ni_{0.43}$LMOs, was successfully fabricated. It exhibits remarkable performance for OER in 0.1 M KOH producing a current density of 10 mA cm^{-2} at an overpotential of 0.34 V (1.57 V *vs*. RHE), better than that of the commercial Ir/C (20 %) catalyst. Simultaneously, good catalytic performance for HER in 0.5 M H_2SO_4 producing a current density of 10 mA cm^{-2} at an overpotential of 52 mV and a Tafel slope of 34 mV dec^{-1}, approaching to that of the commercial Pt/C (20 %) nanocatalyst. Particularly, CFP/$NiCo_2O_4$/$Co_{0.57}Ni_{0.43}$LMOs present better durability under harsh OER and HER cycling conditions than commercial Ir/C and Pt/C. Furthermore, an H-type electrolyzer was fabricated by applying CFP/$NiCo_2O_4$/$Co_{0.57}Ni_{0.43}$LMOs as cathode and anode electrocatalyst, which can be driven by a single-cell battery. This bifunctional catalyst will be very promising in overall water splitting.

Introduction

Due to accelerated depletion of fossil fuels, splitting water into hydrogen and oxygen has attracted great interest in recent years.[1,2] For the water-splitting reaction, both the oxygen evolution reaction (OER) and the hydrogen evolution reaction (HER) are vital for its overall efficiency.[3,4] Usually, the noble metals are used to serve as the efficient catalysts for OER and HER (e.g., Ir or Ru for OER[3] and Pt for HER[4]), but the high cost limits their large-scale application. Therefore, developing efficient and economical catalysts comprised of easily obtained materials for the OER and HER is becoming very crucial for water splitting devices,[5,6] in which the water-splitting catalysts made up of earth-abundant elements have been paid a lot of attention.[7] Recently, synthetic mimics of enzymes based on Fe[8] (hydrogenase active site) and heterogeneous metal oxide systems (e.g.,Co_3O_4 clusters)[9] have been applied in the water splitting, and they show good performance in producing hydrogen and oxygen, respectively. While an interesting and appealing subject being in the ascendant level is how to produce hydrogen and oxygen simultaneously with good yields by using an efficient and distinctive catalyst. Cobo et al. reported a robust nanoparticulate electrocatalytic material (H_2-CoCat) composed of metallic cobalt coated with a cobalt-oxo/hydroxo-phosphate layer in contact with the electrolyte, which shows to be efficient in mediating H_2 evolution from neutral aqueous buffer at modest overpotentials. On the other hand, it is also effective in catalysing O_2 evolution when it was converted on anodic equilibration into the amorphous cobalt oxide film (O_2-CoCat or CoPi).[10a] More recently, a series of water-soluble copper complexes have been investigated by Liu and coworkers, which can be used as catalyst precursors to generate the copper-based bifunctional catalyst for both hydrogen production and water oxidation reactions.[10b] Evidently, these 3d-metal-based catalysts are very promising in the water-splitting process.[11] Noticeably, compounds of AB_2X_4 (A, B = metal, X = chalcogen) as 3d-metal-based catalysts have good efficiency in OER, which can be used as cheap, sustainable and efficient electrocatalyst alternatives to noble metal based materials.[12,13] For instance, $NiCo_2O_4$ shows great effience in OER.[14] It stimulates us to explore whether we can fabricate another bifunctional catalyst based on $NiCo_2O_4$.

It is known that ternary nickel-cobalt metal oxide such as nickel cobaltite ($NiCo_2O_4$) adopts a structure in which nickel occupies the octahedral sites and cobalt distributes over both octahedral and tetrahedral sites,[15,16] and it displays many intriguing advantages like low cost, abundant resources and easy to offer richer redox chemistry because of the

[a]*Key Laboratory of Nonferrous Metal Chemistry and Resources Utilization of Gansu Province, State Key Laboratory of Applied Organic Chemistry and The Research Center of Biomedical Nanotechnology, Lanzhou University, Lanzhou, 730000, P. R. China.*
E-mail: xipx@lzu.edu.cn
[b]*Key Laboratory of Advanced Energy Materials Chemistry (Ministry of Education), Nankai University, Tianjin, 300071, P. R. China.*
[c]*Advanced Ceramic Fibers and Composites laboratory, College of Aerospace Science and Engineering, National University of Defense Technology, Changsha, 410073, P. R. China*
† Footnotes relating to the title and/or authors should appear here.
Electronic Supplementary Information (ESI) available: [details of any supplementary information available should be included here]. See DOI: 10.1039/x0xx00000x

Nanoscale Accepted Manuscript

combinedcontributions from both nickel and cobalt ions.[17] It has been reported that $NiCo_2O_4$ performed better toward OER.[14] To realize the overall water splitting, highly active HER catalysts also need to be developed. Through optimize of the surface structure of electrodes to improve their performance is proved to be a prime method for the fabrication of the electro catalysts.[18] As an example, Hu and co-workers had proved that layered double hydroxide is a kind of efficient electro catalyst.[19] To expand the HER performance of $NiCo_2O_4$, meet the bifunctional requirement and extend the scope of non-precious HER catalysts more active Co and Ni-based layered mixed oxide nanosheets ($Co_{0.57}Ni_{0.43}$LMOs) are desirable candidate for alter the surface of CFP/$NiCo_2O_4$ to achieve the enhanced OER and better HER performance for water splitting.

Results and discussion

Characterization Studies

A two-step strategy was used to fabricate CFP/$NiCo_2O_4$/$Co_{0.57}Ni_{0.43}$LMOs. First, $NiCo_2O_4$ NWs is hydrothermally grown on CFP according our previous method,[20] followed by an electro-deposition, a thin $Co_{0.57}Ni_{0.43}$ DHs were coated on the $NiCo_2O_4$ NWs, and then annealed at 300 °C in air for 2 hours to get the CFP/$NiCo_2O_4$/$Co_{0.57}Ni_{0.43}$LMOs. **Fig. 1a** shows the X-ray diffraction (XRD) patterns for $NiCo_2O_4$ NWs grown on CFP and the $Co_{0.57}Ni_{0.43}$LMOs which were coated on the CFP/$NiCo_2O_4$. From the XRD patterns, we can found that the hybrid structure contains *cubic* $NiCo_2O_4$ with lattice constants a = b =c = 8.11 Å and a space group of *F*3* (JCPDS Card No.20-781). There are two noticeable lattice planes (220) and (311) of $NiCo_2O_4$, which at 2θ of 31.21 and 36.78.[21a] The mixed oxide NiO and Co_3O_4 with rhombohedral and cubic structure, which belong to the space group of *R-3m* (JCPDS Card No. 22-1189) and *Fd3m* (JCPDS Card No. 42-1467), respectively. There are two noticeable lattice planes (220) at 2θ of 43.78 for NiO and (311) at 2θ of 36.78 for Co_3O_4.[21b] **Fig. 1b** shows the scaning electron microscopy (SEM) image illustrates that the $NiCo_2O_4$ NWs which uniform coated on the CFP. The $NiCo_2O_4$ NWs are highly porous and composed of 10-20 nm nanocrystallites with pores of 2-4 nm in diameter (insert of **Fig. 1b**). The transmission electron microscopy (TEM), high-resolution transmission electron microscopy (HRTEM) image and selected area electron diffraction (SAED) pattern show that the mesoporous $NiCo_2O_4$ NWs are polycrystalline (**Fig. S2**). After the coating process, the $Co_{0.57}Ni_{0.43}$LMOs were coated on the CFP/$NiCo_2O_4$ to form CFP/$NiCo_2O_4$/$Co_{0.57}Ni_{0.43}$LMOs, as illustrated in **Fig. 1c**. The $Co_{0.57}Ni_{0.43}$LMOs thin film coatings on the surface of $NiCo_2O_4$ NWs have a thickness of several nanometers which is observed in TEM image (**Fig. 1d**). **Fig. 1e** shows the HRTEM image of amorphous $Co_{0.57}Ni_{0.43}$LMOs which presents different domains and crystalline of $NiCo_2O_4$, with a clearly identified lattice fringe space of 2.4 Å corresponding to the (311) plane of the cubic $NiCo_2O_4$ spinel phase. The spatial distributions of the elements in the shell structures were characterized using energy-dispersive spectroscopy (EDS) in the form of individual elements (Co, Ni, and O) (**Fig. 1f**), together verifying the homogeneous distribution of closely interconnected $NiCo_2O_4$ NWs and layered mixed oxide nanosheets. These results clearly confirm that $NiCo_2O_4$/$Co_{0.57}Ni_{0.43}$LMOs have been successfully prepared.

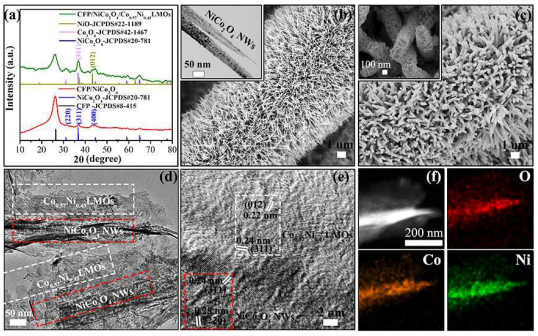

Fig.1 (a) XRD of $NiCo_2O_4$ NWs and CFP/$NiCo_2O_4$/$Co_{0.57}Ni_{0.43}$LMOs. (b) SEM image of CFP/$NiCo_2O_4$ NWs. The oinset in (b) shows the TEM of the $NiCo_2O_4$ NWs. (c) SEM image of CFP/$NiCo_2O_4$/$Co_{0.57}Ni_{0.43}$LMOs. Inset in (c) shows the SEM of the CFP/$NiCo_2O_4$/$Co_{0.57}Ni_{0.43}$LMOs. (d) TEM image of single CFP/$NiCo_2O_4$/$Co_{0.57}Ni_{0.43}$LMOs. (e) HRTEM image of CFP/$NiCo_2O_4$/$Co_{0.57}Ni_{0.43}$LMOs. (f) EDS elemental mapping images of CFP/$NiCo_2O_4$/$Co_{0.57}Ni_{0.43}$LMOs.

Microscopic elemental compositions of $NiCo_2O_4$/$Co_{0.57}Ni_{0.43}$LMOs were further investigated using energy dispersive X-ray (EDX). The EDX measurements show that Co, Ni and O are the component elements of the $NiCo_2O_4$/$Co_{0.57}Ni_{0.43}$LMOs (**Fig. S1**). The chemical compositions of CFP/$NiCo_2O_4$/$Co_{0.57}Ni_{0.43}$LMOs were further analyzed by X-ray photoelectron spectra (XPS). An elemental survey of XPS indicates the presence of Co, Ni, O elements in CFP/$NiCo_2O_4$/$Co_{0.57}Ni_{0.43}$LMOs (**Fig. S3**). The O1s spectra (**Fig. 2a**) show three oxygen contributions, denoted as O1 (529.5 eV), O2 (532.7 eV) and O3 (531.1 eV), corresponding to the three different O in CFP/$NiCo_2O_4$/$Co_{0.57}Ni_{0.43}$LMOs. The Co 2p spectra (**Fig. 2b**) are composed of two spin-orbit doublets characteristic of Co^{2+} and Co^{3+} and two shakeup satellites (identified as "Sat."). Two main peaks observed at 794.81 eV and 779.65 eV with spin-orbit splitting of ~15 eV are attributed to Co $2p_{1/2}$ and Co $2p_{3/2}$. Additionally, there are two shake-up satellite peaks at ~803.38 eV and ~789,35 eV.The energy gap between the Co 2p main peak and the satellite peak is about 9.7 eV, which means the Co cation holds a valence of 3^+.[22] Similarly, the Ni 2p spectra (**Fig. 2c**) consist of two spin-orbit doublets characteristics of Ni^{2+} and Ni^{3+} and two Sat. Two main peaks observed at 872.34 eV and 854.90 eV with spin-orbit splitting of ~17 eV are attributed to Ni $2p_{1/2}$ and Ni $2p_{3/2}$. Additionally, there are two shake-up satellite peaks at ~878.72 eV and ~860.59 eV.[23] Further, Raman spectroscopy was also used to characterize the phase composition of the CFP/$NiCo_2O_4$/$Co_{0.57}Ni_{0.43}$LMOs hybrid structure. As shown in **Fig. S4**, the peaks at 186, 480, 529, and 668 cm^{-1} correspond to F_{2g}, E_g, F_{2g} and A_{1g} models of the $NiCo_2O_4$ NWs, respectively.[24] After $Co_{0.57}Ni_{0.43}$LMOs coating, a new peak at 564 cm^{-1} was observed, corresponding to the well-known A_{1g} models of the Co_3O_4, which the peak at 638 cm^{-1} corresponds to the A_{1g}

Nanoscale Accepted Manuscript

This journal is © The Royal Society of Chemistry 20xx

models of NiO.[25] The above results clearly demonstrate that CFP/$NiCo_2O_4$/$Co_{0.57}Ni_{0.43}$LMOs were successfully fabricated. To investigate the conduction band (CB) and valence band (VB) levels of CFP/$NiCo_2O_4$ and CFP/$NiCo_2O_4$/$Co_{0.57}Ni_{0.43}$LMOs, cyclic voltammetry (CV) analysis was performed with an Ag/AgCl reference electrode (**Fig. S5**).[26] The calculated CB, VB, and electrochemical band gaps of CFP/$NiCo_2O_4$ and CFP/$NiCo_2O_4$/$Co_{0.57}Ni_{0.43}$LMOs (**Table 1**) are similar to the reported band gaps that are suitable for water splitting applications.[27] Furthermore, the bandgap of the CFP/$NiCo_2O_4$/$Co_{0.57}Ni_{0.43}$LMOs have been reduced to 1.02 eV from 1.49 eV of CFP/ $NiCo_2O_4$ after $Co_{0.57}Ni_{0.43}$LMOs coating, which could lead to more charge carriers and higher intrinsic conductivity.[28]

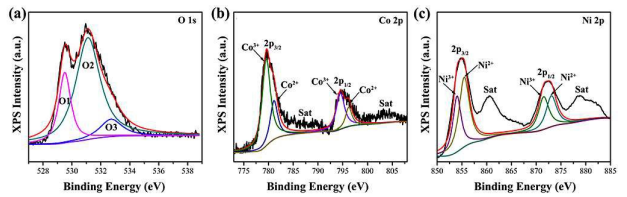

Fig. 2 XPS spectrum of the (a) O 1s, (b) Co 2p and (c) Ni 2p of CFP/$NiCo_2O_4$/$Co_{0.57}Ni_{0.43}$LMOs.

Table 1. The CB and VB of CFP/$NiCo_2O_4$ and CFP/$NiCo_2O_4$/$Co_{0.57}Ni_{0.43}$LMOs.

Catalyst	E_{red} (V)	E_{ox} (V)	E_{CB} (eV)	E_{VB} (eV)	E_g (eV)
CFP/$NiCo_2O_4$	-0.44	0.42	-4.01	-5.5	1.49
CFP/$NiCo_2O_4$/$Co_{0.57}Ni_{0.43}$LMOs	-0.37	0.38	-4.08	-5.1	1.02

Oxygen Evolution Activity

The OER activity of $Co_{0.57}Ni_{0.43}$LMOs was evaluated in O_2-saturated 0.1 M KOH (pH = 13) solution using a standard three-electrode system with a scan rate of 2 mV s^{-1}. Commercial Ir/C catalyst (20 wt% Ir on Vulcan carbon black from Premetek Co.) loading on CFP and CFP were also examined for comparison. The OER polarization curves were recorded by linear sweep voltammetry (LSV) curves, the as-measured reaction currents do not directly reflect the intrinsic behavior of catalysts due to the effect of ohmic resistance (iR), an iR correction was applied to all initial data for further analysis.[29] **Fig. 3a** shows the polarization curves of CFP/$NiCo_2O_4$, CFP/$NiCo_2O_4$/$Co_{0.57}Ni_{0.43}$LMOs, CFP and Ir/C. It can be found that CFP/$NiCo_2O_4$/$Co_{0.57}Ni_{0.43}$LMOs exhibit considerably enhanced OER activity with an onset potential of 1.32 V lower than Ir/C (1.47 V *vs.* RHE), a sharp rise of anodic current resulted from a further positive potential suggests its highly electrocatalytic activity toward the OER. In addition, the overpotential of CFP/$NiCo_2O_4$/$Co_{0.57}Ni_{0.43}$LMOs measured at 10 mA cm^{-2} is 340 mV, which is lower than CFP/$NiCo_2O_4$ (550 mV) and even Ir/C (381 mV) (listed in **Table 2**). Compared to the behaviors of most non-metal[30] and even some metal catalysts like N-doped graphene-$NiCo_2O_4$,[17a] 3D NF/PC/AN,[31] mesoporous Co_3O_4[32] and Co_3O_4/SWNTs[33] in alkaline electrolytes (listed in **Table S1**), this overpotential is more favorable. Furthermore, the OER kinetics of the above catalysts were probed by Tafel plots (log *j* - *η*), more favorable kinetic and superior catalytic activity can be seen from the much lower Tafel slope (**Table 2**). As shown in **Fig. 3b**, the resulted Tafel slopes are found to be 63, 123 and 53 mV dec^{-1} for CFP/$NiCo_2O_4$/$Co_{0.57}Ni_{0.43}$LMOs, CFP/$NiCo_2O_4$ and Ir/C, respectively (**Table 2**), which suggesting that CFP/$NiCo_2O_4$/$Co_{0.57}Ni_{0.43}$LMOs acts as a high-performance anode for generating oxygen from water.

To investigate the reaction mechanism, the rotating ring-disk electrode (RRDE) technique was employed with a Pt ring electrode potential of 1.50 V to oxidize the peroxide intermediates formed at the CFP/$NiCo_2O_4$/$Co_{0.57}Ni_{0.43}$LMOs surface during the OER process. CFP/$NiCo_2O_4$/$Co_{0.57}Ni_{0.43}$LMOs were crushed and coated on a RRDE (see experimental for details). As shown in **Fig. 3c**, a very low ring current (*μ*A scale) was detected, suggesting a desirable four electron pathway without hydrogen peroxide formation for water oxidation (i.e., $4OH^- \rightarrow O_2 + 2H_2O + 4e^-$).[34] Furthermore, an RRDE with a ring potential of 0.40 V was applied to reduce the generated O_2, rendering a continuous OER (disk electrode) → ORR (ring electrode) process to calculate the Faradaic efficiency (**Fig. S6**). With the constant disk current at 127 μA, O_2 molecules generated from the disk electrode by the CFP/$NiCo_2O_4$/$Co_{0.57}Ni_{0.43}$LMOs and sweep across the surrounding Pt ring electrode that is held at 0.4 V (*vs*. RHE). Consequently, a ring current of ~24.75 μA was detected (**Fig. 3d**), which can be attributed to OER with a high Faradaic efficiency of 97.3 % (see detailed calculations in the Experimental Section).

The electrochemical impedance spectroscopy (EIS) analysis of CFP, CFP/$NiCo_2O_4$ and CFP/$NiCo_2O_4$/$Co_{0.57}Ni_{0.43}$LMOs were also performed (**Fig. 3e**). The semicircles in the high- and low-frequency range of the Nyquist plot are attributed to the charge-transfer resistance (R_{CT}) and solution resistance (R_S), which are related to the electro catalytic kinetics and a lower value corresponds to a faster reaction rate.[35] The semicircular diameter in the EIS of CFP/$NiCo_2O_4$ is much larger than that of CFP/$NiCo_2O_4$/$Co_{0.57}Ni_{0.43}$LMOs, the Nyquist plots reveal a remarkable decrease of the charge-transfer resistance (R_{CT}) from 13.5 Ω (CFP/$NiCo_2O_4$) to 5.2 Ω (CFP/$NiCo_2O_4$/$Co_{0.57}Ni_{0.43}$LMOs) (**Table S2**), consistent with the lower overpotential and better OER activity (**Fig. 3a**). These findings suggest that CFP/$NiCo_2O_4$/$Co_{0.57}Ni_{0.43}$LMOs have the fastest charge transfer process among all those catalysts due to the unique structure of nanoporous $NiCo_2O_4$ NWs with hierarchically cobalt-nickel layered mixed oxide nanosheets, which exhibit outstanding OER property.

The stability of the catalysts is always an essential aspect in their property evaluation because the durability is crucial for long-term utilization. Durability study of CFP/$NiCo_2O_4$/$Co_{0.57}Ni_{0.43}$LMOs and commercial Ir/C with LSV measurements were conducted in 0.1 M KOH (pH = 13). After continuous CV scanning, negligible difference between the curves measured at the initial cycle and those going through

Nanoscale Accepted Manuscript

4000 CV cycles, while the durability of commercial Ir/C reduced. Evidently, CFP/$NiCo_2O_4$/$Co_{0.57}Ni_{0.43}$LMOs represents much better durability in the OER (**Fig. 3f**). The chronoamperometric response demonstrates the high stability of CFP/$NiCo_2O_4$/$Co_{0.57}Ni_{0.43}$ LMOs, showing a slight anodic current attenuation of 7.56 % within 6 h, whereas Ir/C displays a 3.66 times larger current attenuation of 27.67 % (the insert of **Fig. 3f**), indicating the apparent advantage of active materials directly grown on conductive substrates in comparison to the post coated catalysts on electrodes.[36]

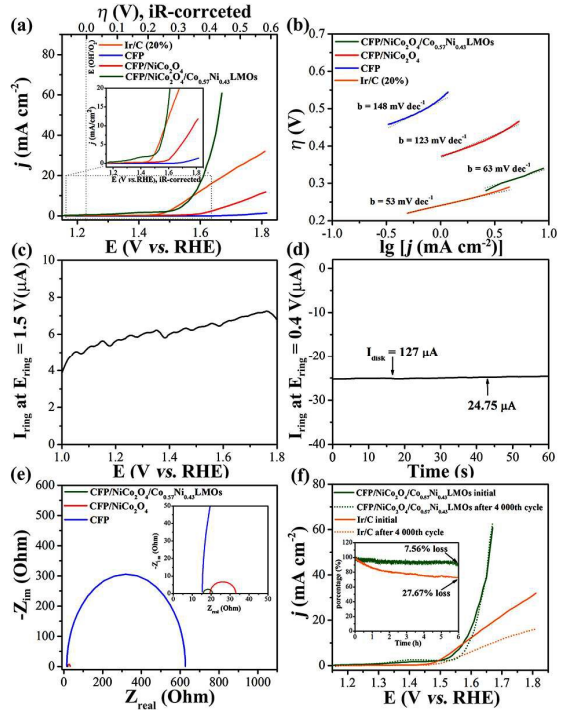

Fig. 3 (a) Linear scan voltammograms (LSV) of CFP/$NiCo_2O_4$, CFP/$NiCo_2O_4$/$Co_{0.57}Ni_{0.43}$LMOs, CFP and Ir/C. The LSV was measured in 0.1 M KOH with a scan rate of 2 mV s^{-1}. (b) Tafel plots (log *j* - *η*) of CFP/$NiCo_2O_4$, CFP/$NiCo_2O_4$/$Co_{0.57}Ni_{0.43}$LMOs, CFP and Ir/C. (c) Ring current of CFP/$NiCo_2O_4$/$Co_{0.57}Ni_{0.43}$LMOs on an RRDE (1600 rpm) in O_2-saturated 0.1 M KOH solution (ring potential 1.50 V). (d) Ring current of CFP/$NiCo_2O_4$/$Co_{0.57}Ni_{0.43}$LMOs on an RRDE (1600 rpm) in N_2-saturated 0.1 M KOH solution (ring potential 0.40 V). (e) Nyquist plots of CFP/$NiCo_2O_4$, CFP/$NiCo_2O_4$/$Co_{0.57}Ni_{0.43}$LMOs and CFP. Inset in (e) shows corresponding Nyquist plot at the high-frequency range. (f) Polarization curves of CFP/$NiCo_2O_4$/$Co_{0.57}Ni_{0.43}$LMOs and Ir/C in 0.1 M KOH before and after 4000 cycles between 1.26 and 1.66 V at a scan rate of 100 mV s^{-1}. The inset in (f) shows chronoamperometric response at a constant potential of 1.52 V.

Meanwhile, after the stability test, there are no obvious changes of CFP/$NiCo_2O_4$/$Co_{0.57}Ni_{0.43}$LMOs from the XRD and XPS results (**Fig. S7** and **Fig. S8**), so the $NiCo_2O_4$/$Co_{0.57}Ni_{0.43}$LMOs are highly OER active and stable. To further evaluate their OER catalytic ability, the mass activity and turnover frequency (TOF) of above catalysts at *η* of 440 mV were also presented (**Table 2**). The calculated mass activity for CFP/$NiCo_2O_4$/$Co_{0.57}Ni_{0.43}$LMOs is 290 A g^{-1}, superior to the CFP/$NiCo_2O_4$. The CFP/$NiCo_2O_4$/$Co_{0.57}Ni_{0.43}$LMOs exhibits the high TOF of 0.0446 s^{-1} than that of Ir/C (0.03744 s^{-1}), implying that the metal atom on the crystal surface was catalytically active.[37] These results indicate that CFP/$NiCo_2O_4$/$Co_{0.57}Ni_{0.43}$LMOs can serve as an effective catalyst for water oxidation.

Hydrogen Evolution Activity

The HER performance of the CFP/$NiCo_2O_4$/$Co_{0.57}Ni_{0.43}$LMOs were carried out using a three-electrode system in 0.5 M H_2SO_4 (pH = 0) with a scan rate of 2 mV s^{-1}. Commercial Pt/C catalysts (20 wt% Pt on Vulcan carbon black from Premetek Co.) loading on CFP and CFP were also examined for comparison. From the LSV curves in **Fig. 4a**, the Pt/C exhibits the HER performance with negligible onsetpotential, while the bare CFP shows little HER activity. The CFP/$NiCo_2O_4$/$Co_{0.57}Ni_{0.43}$LMOs exhibit current densities 10 mA cm^{-2} at an overpotential of 52 mV, whereas CFP/$NiCo_2O_4$ electrode needs an overpotential of 521.7 mV to reach to a current density of 10 mA cm^{-2}. It suggests that CFP/$NiCo_2O_4$/$Co_{0.57}Ni_{0.43}$LMOs acts as a high-performance cathode for HER. In addition, this electrode needs an overpotential of 125 mV to drive current densities of 100 mA cm^{-2}. These overpotentials are more favorable compared to most reported values for non-Pt HER catalysts in acidic aqueous media (**Table S3**). **Fig. 4b** shows the iR-corrected Tafel plots. The linear portions of the Tafel plots are fitted to the Tafel equation ($\eta = b \log j + a$, where *j* is the current density, b is the Tafel slope, and a the intercept relative to the exchange current density j_0),[17] which yields Tafel slopes of 30, 34, 166 and 225 mV dec^{-1} for Pt/C, CFP/$NiCo_2O_4$/$Co_{0.57}Ni_{0.43}$LMOs, CFP/$NiCo_2O_4$, and CFP, respectively. The Pt/C exhibits a Tafel slope of ~30 mV dec^{-1} and an exchange current density of 0.71 mA cm^{-2}, which is consistent with the reported value.[38] The Tafel slopes for CFP/$NiCo_2O_4$/$Co_{0.57}Ni_{0.43}$LMOs catalysts do not match the expected Tafel slopes of 39 mV dec^{-1}, which reveals that the HER proceeds via a Volmer-Heyrovsky mechanism.[39] For hydrogen evolution in acid solutions on metal electrode surfaces using CFP/$NiCo_2O_4$/$Co_{0.57}Ni_{0.43}$LMOs, the mechanism typically involves three major reactions.[40]

Table 2. Comparison of OER activity data for different catalysts

Catalyst	Onset potential [V *vs*. RHE]	*η* at *J* = 10 mA cm^{-2} [mV]	Tafel slope (mV dec^{-1})	TOF at *η* = 440 mv s^{-1}	Mass activity at *η* = 440 mv s^{-1}
CFP	1.63		148		
CFP/ $NiCo_2O_4$	1.52	550	123	0.00228	4.42
CFP/$NiCo_2O_4$/$Co_{0.57}Ni_{0.43}$LMOs	1.32	340	63	0.0446	290.00
Ir/C (20%)	1.47	381	53	0.03744	375.86

Nanoscale Accepted Manuscript

This journal is © The Royal Society of Chemistry 20xx

H_3O^+ + e-catalyst ↔H-catalyst + H_2O
(Volmer reaction, Tafel slope 120 mV dec^{-1}) **(1)**
2-H catalyst↔ H_2-catalyst
(Tafel reaction, Tafel slope 30 mV dec^{-1}) **(2)**
H_3O^+ + e-catalyst + H-catalyst↔H_2-catalyst + catalyst + H_2O
(Heyrovsky reaction, Tafel slope 40 mV dec^{-1}) **(3)**

In these reactions processes, e-catalyst denotes metal-bound electrons, and H-catalyst and H_2-catalyst represent a hydrogen atom and a hydrogen molecule adsorbed on to a surface metal atom, respectively. These reactions are dependent on the inherent (electro) chemical and electronic properties of the catalyst surface. Two main pathways are generally observed for HER, Volmer-Tafel reaction (**eqs 1 and 2**) and Volmer-Heyrovsky reaction (**eqs 1 and 3**). In the present study, the Tafel slope of 34 mV dec^{-1} for CFP/$NiCo_2O_4$/$Co_{0.57}Ni_{0.43}$LMOs suggests that HER is likely controlled by both the first-electron reduction of protons and electrochemical desorption of hydrogen (Volmer-Heyrovsky reaction). The exchange current density (j_0) of CFP/$NiCo_2O_4$/$Co_{0.57}Ni_{0.43}$LMOs is calculated to be 0.21 mA cm^{-2}, 44 times larger than that of CFP/$NiCo_2O_4$ (**Table 3, Fig. S9**).

To investigate the electrode kinetics under HER process, the EIS measurements for CFP, CFP/$NiCo_2O_4$ and CFP/$NiCo_2O_4$/$Co_{0.57}Ni_{0.43}$LMOs were carried out ranging from 100 MHz to 0.01 Hz (**Fig. 4c**). The semicircles in the high- and low-frequency range of the Nyquist plot attributed to the charge-transfer resistance (R_{CT}) and solution resistance (R_S), respectively, are related to the electrocatalytic kinetics and a lower value corresponds to a faster reaction rate.[31] Similarly, smaller R_{CT} of 4.5 Ω is realized on CFP/$NiCo_2O_4$/$Co_{0.57}Ni_{0.43}$LMOs compared to CFP/$NiCo_2O_4$ (189.3 Ω) (**Table S4**), consistent with the lower overpotential. The superior activity of CFP/$NiCo_2O_4$/$Co_{0.57}Ni_{0.43}$LMOs for HER may arise from the nanoporous $NiCo_2O_4$ NWs with cobalt-nickel layered mixed oxide nanosheets, which could yield easier mass transportation.[41] Also, such a decrease of the EIS of the Nyquist plots can be attributed to the enhancement of interdomain conductivity.

The durability of CFP/$NiCo_2O_4$/$Co_{0.57}Ni_{0.43}$LMOs was also examined. As shown in **Fig. 4d**, after continuous CV scanning for 10000 cycles in 0.5 M H_2SO_4 at a scan rate of 100 mV s^{-1}, the polarization curve shows negligible difference compared with the initial one. To further understand the stability of the hybrid catalysts, SEM, XRD and XPS of CFP/$NiCo_2O_4$/$Co_{0.57}Ni_{0.43}$LMOs electrode after durability test were evaluated (**Fig. S10**, **Fig. S11** and **Fig. S12**). It is found that there is no obvious deformation of perpendicularly-oriented CFP/$NiCo_2O_4$/$Co_{0.57}Ni_{0.43}$LMOs heterostructure after the durability test. The durability study suggests that the CFP/$NiCo_2O_4$/$Co_{0.57}Ni_{0.43}$LMOs electrode is inherently stable for HER because both $NiCo_2O_4$ NWs and $Co_{0.57}Ni_{0.43}$LMOs are produced in situ.

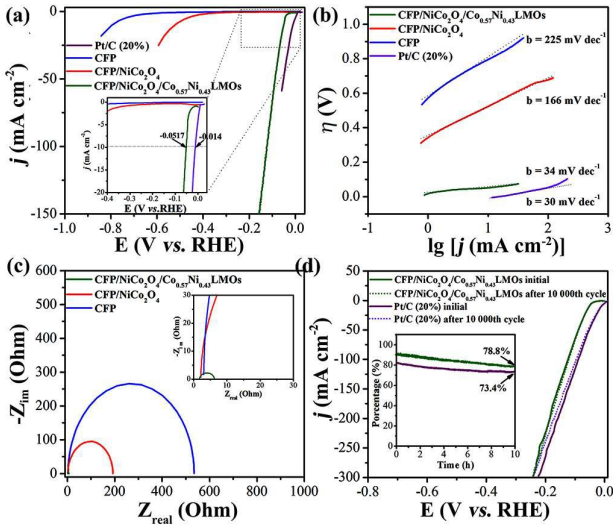

Fig. 4 (a) Polarization curves of CFP/$NiCo_2O_4$, CFP/$NiCo_2O_4$/$Co_{0.57}Ni_{0.43}$LMOs, CFP and Pt/C in 0.5 M H_2SO_4 with a scan rate of 2 mV s^{-1}. (b) Tafel plots of CFP/$NiCo_2O_4$, CFP/$NiCo_2O_4$/$Co_{0.57}Ni_{0.43}$LMOs, CFP and Pt/C. (c) Nyquist plots of different samples. Inset in (c) shows corresponding Nyquist plot at the high-frequency range. (d) Polarization curves for CFP/$NiCo_2O_4$/$Co_{0.57}Ni_{0.43}$LMOs before and after of 10000 cycles between -0.23 V and +0.22 V *vs.* RHE at a scan rate of 100 mV s^{-1} in 0.5 M H_2SO_4.

To gain further insight into the intrinsic catalytic activity of CFP/$NiCo_2O_4$/$Co_{0.57}Ni_{0.43}$LMOs, the turnover frequency (TOF) for each active site was estimated using the methods reported previously.[42] The number of active sites was first examined by CV in phosphate buffer (pH = 7) at a scan rate of 50 mV s^{-1}. The number of active sites on the catalyst modified GCE was calculated to be 3.55×10^{-8} mol. The calculated TOF are shown in **Fig. S13**. As the most active catalyst, Pt shows a TOF of 0.8 s^{-1} at η = 0 mV.[43] To achieve a TOF of 0.752 s^{-1}, CFP/$NiCo_2O_4$/$Co_{0.57}Ni_{0.43}$LMOs need an overpotential of ~46 mV, much smaller than that of defect-rich MoS_2 (300 mV).[44] To reach a TOF of 4 s^{-1}, the CFP/$NiCo_2O_4$/$Co_{0.57}Ni_{0.43}$LMOs electrode needs an overpotential of 70 mV, 170 mV smaller than self-supported nanoporous CoP nanowire arrays (240 mV).[45] Potentiostatic cathodic electrolysis was performed by maintaining CFP/$NiCo_2O_4$/$Co_{0.57}Ni_{0.43}$LMOs at an overpotential of 300 mV for 60 minutes. By comparing the amount of measured hydrogen with calculated hydrogen (assuming 100 % FE), we observed a FE close to 100 % for the hydrogen evolution (**Fig. 5**).

Table 3. Comparison of HER activity data for different catalysts.

Catalyst	Onset potential [mV *vs.*RHE]	η at J = 10 mA cm^{-2} [mV]	Tafel slope (mV dec^{-1})	Exchange current density (mA cm^{-2})
CFP	244.5	793	225	2.4×10^{-3}
CFP/$NiCo_2O_4$	149	521.7	166	4.8×10^{-3}
CFP/$NiCo_2O_4$/$Co_{0.57}Ni_{0.43}$LMOs	29	52	34	0.21
Pt/C (20%)	0	14	30	0.71

Nanoscale Accepted Manuscript

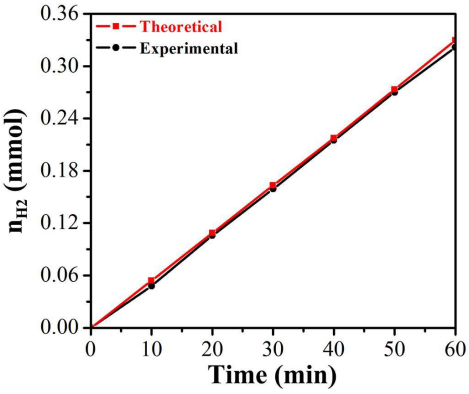

Fig. 5 The amount of theoretically calculated (red line) and experimentally measured (black line) hydrogen versus time for CFP/$NiCo_2O_4$/$Co_{0.57}Ni_{0.43}$LMOs at -0.3 V for 60 min.

Bifunctional Performance for OER and HER

Based on the above explanations, it can be concluded that CFP/$NiCo_2O_4$/$Co_{0.57}Ni_{0.43}$LMOs are highly efficient, noble-metal-free bifunctional electrocatalysts for OER and HER. The CFP/$NiCo_2O_4$/$Co_{0.57}Ni_{0.43}$LMOs can be used for both OER and HER in the same electrochemical cell under pH change between 0 and 13 (**Fig. 6**). The current density for OER performed at 0.804 V (1 h) is 7.3 mA cm^{-2}. Then the applied potential was switched to -0.347 V for HER in 0.5 M H_2SO_4, the current density is 5.3 mA cm^{-2}. Obviously, the CFP/$NiCo_2O_4$/$Co_{0.57}Ni_{0.43}$LMOs are highly efficient and good stability during water splitting.

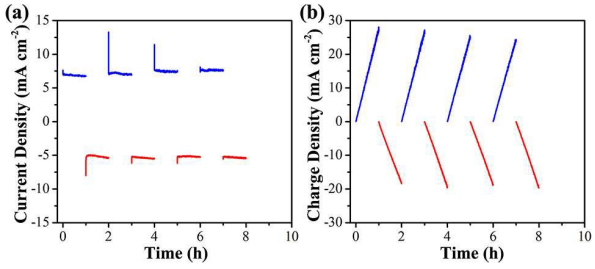

Fig. 6 (a) Current density and (b) charge density change when CFP/$NiCo_2O_4$/$Co_{0.57}Ni_{0.43}$LMOs used as a function of OER and HER bifunctional electro catalyst for water splitting. CFP/$NiCo_2O_4$/$Co_{0.57}Ni_{0.43}$LMOs used for OER was performed at +0.804 V for 1 h, and then the applied potential was switched to -0.347 V for HER.

As previously mentioned, oxygen vacancies play an important role in the OER.[46] Similarly, for $Co_{0.57}Ni_{0.43}$LMOs, they possess rich oxygen vacancies, which were confirmed by XPS. In the O 1s core level spectra, three peaks were clearly identified (**Fig. 7a**). The peak at 529.5 eV is due to oxygen atoms bound to metals,[47] the peak at 532.7 eV is associated with hydroxyl species of surface-adsorbed water molecules,[48] and the peak at 531.1 eV is attributed to a high number of defect sites with a low oxygen coordination.[49] The area for the peak at 531.1 eV is the largest for the CFP/$NiCo_2O_4$/$Co_{0.57}Ni_{0.43}$LMOs, indicating that $Co_{0.57}Ni_{0.43}$LMOs obtained in the air possess more oxygen vacancies than the other counterparts. The chemical synergistic effect between the $Co_{0.57}Ni_{0.43}$LMOs and $NiCo_2O_4$ also contributes to the enhanced activity. **Fig. 7b** shows that the electron-binding energy of Co 2p in $NiCo_2O_4$ decreases by 0.2 eV after being decorated by $Co_{0.57}Ni_{0.43}$LMOs. This is probably caused by the electron transfer from the $Co_{0.57}Ni_{0.43}$LMOs to the $NiCo_2O_4$ NWs. The more Lewis acidic $Co_{0.57}Ni_{0.43}$LMOs further facilitates the activation of Lewis basic H_2O through Lewis acid-base interaction, which finally leads to an improved activity for the HER.[37]

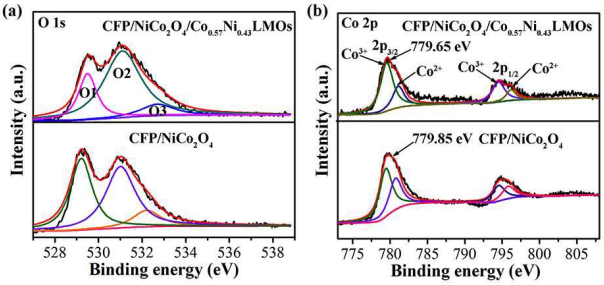

Fig. 7 (a) High-resolution O 1s XPS spectra for CFP/$NiCo_2O_4$ and CFP/$NiCo_2O_4$/$Co_{0.57}Ni_{0.43}$LMOs. (b) High-resolution Co 2p XPS spectra for CFP/$NiCo_2O_4$ and CFP/$NiCo_2O_4$/$Co_{0.57}Ni_{0.43}$LMOs.

Finally, an H-type water electrolyzer was fabricated by applying CFP/$NiCo_2O_4$/$Co_{0.57}Ni_{0.43}$LMOs as the water reduction catalyst in 0.5 M H_2SO_4 and as the water oxidation catalyst in 0.1 M KOH which is separated by proton exchange membranes (Nafion 117) (**Fig. 8a**).[50] This H-type water electrolyzer performed a current density of 1.47 mA cm^{-2} (25 °C) at 1.5 V and 4.62 mA cm^{-2} (60 °C) at 1.5 V (**Fig. 8b**). Such H-type water electrolyzer can be drived by a single-cell AA battery with a voltage of 1.5 V (**Fig. 8a** and see Supplementary Movie 1 for a video of water electrolysis by an AA battery). Excitingly, a voltage of 1.5 V for overall water splitting using non-precious catalysts for both electrodes was successfully achieved, in which the CFP/$NiCo_2O_4$/$Co_{0.57}Ni_{0.43}$LMOs catalyst can be used as a bifunctional catalyst for efficient electrolyzers with ultralow overpotential for water-splitting devices.

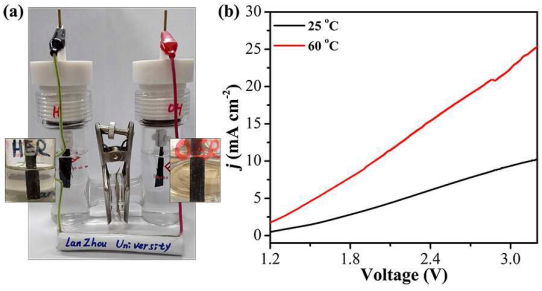

Fig. 8 (a) Optical photograph of the water-splitting device powered by an AA battery with a voltage of 1.5 V showing the generation of hydrogen and oxygen bubbles on CFP/$NiCo_2O_4$/$Co_{0.57}Ni_{0.43}$LMOs. (b) Polarization curves of electrolyzer using CFP/$NiCo_2O_4$/$Co_{0.57}Ni_{0.43}$LMOs as HER in 0.5 M H_2SO_4 and OER catalyst in 0.1 M KOH under different temperature.

From the above results and discussions, we can find that the as-prepared CFP/$NiCo_2O_4$/$Co_{0.57}Ni_{0.43}$LMOs can be applied as

Nanoscale Accepted Manuscript

This journal is © The Royal Society of Chemistry 20xx

an efficient catalyst for overall water splitting because: (1) the excellent OER performance is originated from the $Co_{0.57}Ni_{0.43}$LMOs on 3D CFP/$NiCo_2O_4$ NWs structure with rich oxygen vacancies, which can maximize the exposure of their edge sites at the atomic scale and present a superior catalysis activity for oxygen production; (2) the outstanding HER performance is attributed to the compact configuration of the $Co_{0.57}Ni_{0.43}$LMOs anchored onto the nanoporous CFP/$NiCo_2O_4$ NWs; the in situ incorporated carbon (from CFP) causes the impaired electron density of Co atoms, which can make the catalytically active species more nucleophilic and thus facilitate the adsorption and reaction of H^+ groups with $NiCo_2O_4$/$Co_{0.57}Ni_{0.43}$LMOs with enhanced HER activity in acid solutions; (3) these layered mixed oxide nanosheets: $Co_{0.57}Ni_{0.43}$LMOs promotes the conductivity of NWs and offers rich accessible electro-active sites, short ion transport pathways, and superior electron collection efficiency and buffer the large volume change during the fast charging-discharging process; (4) The direct growth of active materials on CFP can greatly enhance the electron transport and adhesion between nanowire arrays and substrates, promote the structural stability and avoid utilization of polymeric binders, leading to excellent water splitting activity and stronger durability in comparison to those of commercial Ir/C and Pt/C nanocatalysts.

Conclusions

In summary, the nanostructured $NiCo_2O_4$/$Co_{0.57}Ni_{0.43}$LMOs attached to CFP network has been developed as a highly efficient bifunctional catalyst for both OER and HER. The CFP/$NiCo_2O_4$/$Co_{0.57}Ni_{0.43}$LMOs exhibit OER performance better than the commercial Ir/C, while the HER performance is comparable to that of Pt/C catalyst. Particularly, CFP/$NiCo_2O_4$/$Co_{0.57}Ni_{0.43}$LMOs presents good durability under harsh OER and HER cycling conditions than commercial Ir/C and Pt/C catalyst, respectively. The overall water splitting performance of CFP/$NiCo_2O_4$/$Co_{0.57}Ni_{0.43}$LMOs is the best among all the reported nanowire array electrodes and is better than that of most of the highly active noble-metal/transition-metal and nonmetal water splitting catalysts. The excellent water splitting performance can be attributed to the porous nanowire array electrode configuration and in situ $Co_{0.57}Ni_{0.43}$LMOs incorporation which inducing the rich oxygen vacancies and electron transfer from the $Co_{0.57}Ni_{0.43}$LMOs to the $NiCo_2O_4$ NWs, leading to strong structural stability, and improved mass/charge transport. Therefore, CFP/$NiCo_2O_4$/$Co_{0.57}Ni_{0.43}$LMOs can serve as a promising noble-metal-free catalyst as anode and cathode for splitting water into H_2 and O_2, which have potential application in overall water splitting.

EXPERIMENTAL SECTION

Chemicals and Materials

Nickel nitrate hexahydrate (98.0 %), cobalt (II) nitrate hexahydrate (99.0 %), urea (99.0 %), potassium hydroxide (90.0 %), sulfuric acid (95.0 %) were purchased from Aladdin. Rod GCEs were from the Chen hua Co. Ltd. (Shanghai, China). The demonized (DI) water for solution preparation was from a Millipore Autopure system (18.2 MΩ, Millipore Ltd., USA). The 0.1 M KOH and 0.5 M H_2SO_4 and was employed as a supporting electrolyte in the electrochemical experiment. Commercial carbon fiber papers (CFP) were purchased from Fuel Cell Store. Nafion 117 (brand: Dupont) was purchased from Shanghai Hesen Electrical Co., Ltd. All the other Chemicals and reagents for electrochemical measurements were of analytical grade and used as received.

Structural Characterizations

The morphologies of the samples were investigated using field-emission scanning electron microscopy (FESEM, Zeiss) at an acceleration voltage of 5 kV. All samples were coated with a thin layer of gold prior to FESEM observations. The chemical compositions were investigated by the energy dispersive X-ray spectroscopy (EDX). Transmission electron microscopy (TEM) and high-resolution transmission electron microscopy (HRTEM) observations were performed under an acceleration voltage of 200 kV with a JEOL JEM 2100 TEM. Sample compositions were determined by ICP-AES (HITACHI P-4010, Japan). X-ray diffraction (XRD) experiments were conducted 2θ from 10^o to 80^o on an X'Pert Pro X-ray diffractometer with Cu Ka radiation (λ = 0.1542 nm) under a voltage of 40 kV and a current of 40 mA. X-ray photoelectron spectroscopy (XPS) analyses were made with a VG ESCALAB 220I-XL device. All XPS spectra were corrected using C1s line at 284.6 eV.

Preparation of CFP/$NiCo_2O_4$/$Co_{0.57}Ni_{0.43}$LMOs

First, self-supported $NiCo_2O4$ NWs were prepared by a facile hydrothermal synthesis method.[20] Generally speaking 0.4145 g $Co(NO_3)_2{\cdot}6H_2O$, 0.2063 g $Ni(NO_3)_2{\cdot}6H_2O$, and 0.15 g urea were dissolved in 50 mL DI water. After stirred for about 10 min, a transparent pink colored solution was obtained. Then solution was transferred into a 80mL Teflon-lined stainless steel autoclave. Two pieces of carbon fiber paper (CFP) (3 x $4cm^2$) vertically insert into the Teflon holder were subsequently soaked in the solution following by heated the solution to 120°C in an electric oven, and kept at that temperature for 16h. The as synthesized electrodes were then taken out, ultrasonically cleaned for 5mins in the DI water and rinse with ethanol several times, dried at 80°C over night, and annealed at 300 °C in air for 2 hours to get the $NiCo_2O_4$ nanowire on the CFP. Then, the self-supported $NiCo_2O_4$ NWs were used as the scaffold for $Co_{0.57}Ni_{0.43}$LMOs nanosheet shell growth through a simple cathodic electro-deposition method. The electrolyte for electrodeposition of $Co_{0.57}Ni_{0.43}$LMOs was placed in 70 ml of 0.1 M solution which Ni^{2+}/Co^{2+} concentration ratio is 1:1, and then deposited by the potential static with -1.0 V 15 mins. The substrates were taken off and rinsed with DI water ethanol several times, and annealed at 300 °C in air for 2 hours to get CFP/$NiCo_2O_4$/$Co_{0.57}Ni_{0.43}$LMOs.

Nanoscale Accepted Manuscript

OER Electrocatalytic Research

Electrochemical measurements were carried out in a typical three-electrode glass cell connected to a CHI 760 E Electrochemical Workstation (CHI Instruments, Shanghai Chenhua Instrument Corp., China) at a scan rate of 2 mV s^{-1} in an electrolyte solution of 0.1 M KOH. The synthesized CFP/$NiCo_2O_4$ and CFP/$NiCo_2O_4$/$Co_{0.57}Ni_{0.43}$LMOs were directly used as the working electrode for electrochemical characterizations. The potentials were referenced to the reversible hydrogen electrode (RHE) through RHE calibration in 0.1 M KOH (pH = 13), $E_{(RHE)} = E_{(Ag/AgCl)} + 0.96$ V. Potentials are reported *vs.* Ag/AgCl reference electrode, and a Pt net was employed as an auxiliary electrode. Also, a resistance test was made and the iR compensation was applied by using the CHI software. LSV was conducted in 0.1 M KOH with a scan rate of 2 mV s^{-1}. Onset potentials were determined based on the beginning of the linear regime in the Tafel plot. The time dependency of catalytic currents during electrolysis for the catalyst was tested in 0.1 M KOH at η = 200 mV after equilibrium. In this work, all electrochemical experiments were carried out at 20 ± 0.2 °C. Ir/C catalysts were prepared by dispersing 2 mg of Ir/C (20 wt% Ir on Vulcan XC-72) in 500 µL of EtOH with 17.5 µL of 5 wt% Nafion solution.[52] Then 300 µL of the catalyst ink was loaded onto CFP surface (0.5× 0.5 cm^2) and air-dried at room temperature.

HER Electrocatalytic Research

Electrochemical measurements were carried out in a typical three-electrode glass cell connected to a CHI 760 E Electrochemical Workstation (CHI Instruments, Shanghai Chenhua Instrument Corp., China) at a scan rate of 2 mV s^{-1} in an electrolyte solution of 0.5 M H_2SO_4. The synthesized CFP/$NiCo_2O_4$ and CFP/$NiCo_2O_4$/$Co_{0.57}Ni_{0.43}$LMOs were directly used as the working electrode for electrochemical characterizations. Saturated Ag/AgCl (in a saturated KCl solution) was employed as a reference electrode, and a Pt net was employed as an auxiliary electrode. Also, a resistance test was made and the iR compensation was applied by using the CHI software. In 0.5 M H_2SO_4, the Ag/AgCl electrode was calibrated with respect to reversible hydrogen electrode (RHE): $E_{RHE} = E_{Ag/AgCl} + 0.197$ V. Linear sweep voltammetry (LSV) was conducted in 0.5 M H_2SO_4 with a scan rate of 2 mV s^{-1}. The time dependency of catalytic currents during electrolysis for the catalyst was tested in 0.5 M H_2SO_4 at η = 200 mV after equilibrium. In this work, all electrochemical experiments were carried out at 20 ± 0.2 °C. Pt/C catalysts were prepared by dispersing 2 mg of Pt/C (20 wt% Pt on Vulcan XC-72) in 500 µL of EtOH with 17.5 µL of 5 wt% Nafion solution.[52] Then 300 µL of the catalyst ink was loaded onto CFP surface (0.5 × 0.5 cm^2) and air-dried at room temperature.

Determination of Bandgap

To investigate the conduction band (CB) and valence band (VB) levels of CFP/$NiCo_2O_4$/$Co_{0.57}Ni_{0.43}$LMOs, cyclic voltammograms (CV) analysis was performed with an Ag/AgCl reference electrode. And the ferrocene/ferrocenium redox couple (F_c/F_c^+, -4.8 eV) was used as the reference material for all the CV measurements. The oxidation potential onset of ferrocene as marked by the vertical dotted line (**Figure S5**) is estimated to be 0.35 V (*vs.* Ag/AgCl). Using ferrocene as the reference material, the CB and VB energy levels of the CFP/$NiCo_2O_4$ and CFP/$NiCo_2O_4$/$Co_{0.57}Ni_{0.43}$LMOs can be calculated by the following equation:[51]

$$E_{CB/VB} = - [(E_{red/ox} - E_{ferrocene}) + 4.8] \text{ eV}$$

RRDE measurements and Faradaic efficiency (FE)

To investigate the reaction mechanism for OER, rotating ring-disk electrode (RRDE) voltammograms were conducted on a RRDE configuration (RRDE-3A, Japan) consisting of a glassy carbon disk electrode and a Pt ring electrode. The CFP/$NiCo_2O_4$/$Co_{0.57}Ni_{0.43}$LMOs was crushed and coated on a RRDE using Nafion as the binder. A scan rate of 2 mV s^{-1} and a rotation rate of 1600 rpm were applied for RRDE tests. Specifically, in order to determine the reaction pathway for OER by detecting the HO_2^- formation, the ring potential was held constantly at 1.5 V (*vs.* RHE) for oxidizing HO_2^- intermediate in O_2-saturated 0.1 M KOH; on the other hand, to ensure that the oxidation current originates from oxygen evolution rather than other side reactions and to calculate the Faradaic efficiency of the system, the ring potential was held constantly at 0.40 V(*vs.* RHE) to reduce the O_2 formed from the catalyst on the disk electrode in N_2-saturated 0.1 M KOH solution. The Faradaic efficiency (ε) was calculated as follows:

$$\varepsilon = I_r/(I_d N)$$

where I_d denotes the disk current, I_r denotes the ring current, and N denotes the current collection efficiency of the RRDE. To properly calculate the Faradaic efficiency of the system, the disk electrode was held at a relatively small constant current of 127 µA (~1 mA cm^{-2}); this current is sufficiently large to ensure an appreciable O_2 production and sufficiently small to minimize local saturation and bubble formation at the disk electrode.[34]

H-type water electrolyzer measurement

Furthermore, in order to prove the good performance of CFP/$NiCo_2O_4$/$Co_{0.57}Ni_{0.43}$LMOs for water splitting a H-type water electrolyzer was fabricated which is separated by proton exchange membranes (Nafion 117). A typical two-electrode glass cell connected to a CHI 760 E Electrochemical Workstation. The temperature of this H-type water electrolyzer was adjusted through a water bath. Polarization curves of electrolyzer using CFP/$NiCo_2O_4$/$Co_{0.57}Ni_{0.43}$LMOs as both cathode and andoe in 0.5 M H_2SO_4 and 1.0 M KOH at a scan rate of 2 mV s^{-1} from 1.2 V to 3.3 V. [50]

Active sites calculation

The number of active sites (n) is examined using CVs with phosphate buffer (pH = 7) at a scan rate of 50 mV s^{-1}. When the number of voltammetric charges (Q) is obtained after deduction of the blank value, n (mol) can be calculated with the following equation:[35]

Nanoscale Accepted Manuscript

This journal is © The Royal Society of Chemistry 20xx

$$n = Q/2F$$

where F is Faraday constant (96480 C mol^{-1}). For the sample of CFP/$NiCo_2O_4$/$Co_{0.57}Ni_{0.43}$LMOs, Q is 3.347×10^{-2} C, n (mol) = $3.347\times10^{-2}/(2\times96480)$ mol = 1.73×10^{-7} mol. Turnover frequency (TOF, s^{-1}) is calculated with the following equation: [52]

$$TOF = I/(2Fn)$$

where I (A) is the current of the polarization curve obtained from the LSVs measurements.

Acknowledgements

We acknowledge support from the National Natural Science Foundation of China (No. 21571089, 21201092, 21403097, 51203184 and 21501081), National Fund for Talent Training in Basic Science of China (No. J1103307), the Research Fund for the Doctoral Program of Higher Education (No. 20120211120020) and the Fundamental Research Funds for the Central Universities (Lzujbky-2014-m02, Lzujbky-2015-19 and lzujbky-2014-182).

Notes and references

1 (*a*) T. R. Cook, D. K. Dogutan, S. Y. Reece, Y. Surendranath, T. S. Teets and D. G. Nocera, *Chem. Rev.*, 2010, **110**, 6474-6502; (*b*) M. G. Walter, E. L. Warren, J. R. McKone, S. W. Mi, Q. X. Boettcher, E. A. Santori and N. S. Lewis, *Chem. Rev.*, 2010, **110**, 6446-6473.

2 (*a*) J. Kibsgaard, Z. B. Chen, B. N. Reinecke and T. F. Jaramillo, *Nat. Mater*., 2012, **11**, 963-969; (*b*) S. B. Yang, Y. J. Gong, J. S. Zhang, L. Zhan, L. L. Ma, Z. Y. Fang, R. Vajtai, X. C. Wang and P. M. Ajayan, *Adv. Mater*., 2013, **25**, 2452-2456; (*c*) H. M. Chen, C. K. Chen, R. S. Liu, L. Zhang, J. J. Zhang and D. P. Wilkinson, *Chem. Soc. Rev*., 2012, **41**, 5654-5671.

3 (*a*) Q. Yin, J. M. Tan, C. Besson, Y. V. Geletii, D. G. Musaev, A. E. Kuznetsov, Z. Luo, K. I. Hardcastle, and C. L. Hill, *Science*, 2010, **328**, 328-342; (*b*) M. W. Kanan and D. G. Nocera, *Science*, 2008, **321**, 1072-1075.

4 (*a*) D. Merki and X. Hu, *Energy Environ. Sci*., 2011, **4**, 3878-3888; (*b*) H. B. Gray, *Nature Chem*., 2009, **1**,7.

5 (*a*) J. B. Gerken, J. G. McAlpin, J. Y. C. Chen, M. L. Rigsby, W. H. Casey, R. D. Britt and S. S. Stahl, *J. Am. Chem. Soc*., 2011, **133**, 14431-14442; (*b*) Y. Gorlin and T. F. Jaramillo, *J. Am. Chem. Soc.*, 2010, **132**, 13612-13614; (*c*) Y. Y. Liang, Y. G. Li, H. L. Wang, J. G. Zhou, J. Wang, T. Regier and H. J. Dai, *Nat. Mater*., 2011, **10**, 780-786; (*d*) B. S. Yeo and A. T. Bell, *J. Am. Chem. Soc.*, 2011, **133**, 5587-5593; (*e*) D. M. Robinson, Y. B. Go, M. Greenblatt and G. C. Dismukes, *J. Am. Chem. Soc.*, 2010, **132**, 11467-11469.

6 (*a*) E. J. Popczun, C. G. Read, C. W. Roske, N. S. Lewis and R. E. Schaak, *Angew. Chem. Int. Ed.*, 2014, **126**, 5531-5534; (*b*) M.G. Mavros, T. Tsuchimochi, T. Kowalczyk, A. McIsaac, L-P. Wang and T. V. Voorhis, *Inorg. Chem*., 2014, **53**, 6386-6397; (c) S. B. Wang, Y. D. Hou, S. Lin and X. C. Wang, *Nanoscale* 2014, **6**, 9930-9934.

7 (*a*) N. S. Lewis and D. G. Nocera, *Proc. Natl. Acad. Sci. U. S. A.*, 2006, **103**, 15729-15735; (*b*) P. Du and R. Eisenberg, *Energy Environ. Sci*., 2012, **5**, 6012-6021.

8 T. J. Meyer, *Nature*, 2008, **451**, 778-779.

9 F. Jiao and H. Frei, *Angew. Chem. Int. Ed.*, 2009, **48**, 1841-1844.

10 (*a*) S. Cobo, J. Heidkamp, P.-A. Jacques, J. Fize, V. Fourmond, L. Guetaz, B. Jousselme, V. Ivanova, H. Dau, S. Palacin, M. Fontecave and V. Artero, *Nat. Mater*., 2012, **11**, 802-807; (*b*) X. Liu, H. Zheng, Z. Sun, A. Han and D. Du, *ACS Catal*., 2015, **5**, 1530-1538.

11 D. M. Robinson, Y. B. Go, M. Mui, G. Gardner, Z. Zhang, D. Mastrogiovanni, E. Garfunkel, J. Li, M. Greenblatt and G. C. Dismukes, *J. Am. Chem. Soc*., 2013, **135**, 3494-3501.

12 F. Cheng, J. Shen, B. Peng, Z. Tao and J. Chen, *Nat. Chem*., 2011, **3**, 79-84.

13 (*a*) H. L. Wang, Q. M. Gao and L. Jiang, *Small*, 2011, **7**, 2454-2459; (*b*) T. Y. Wei, C. H. Chen, H. C. Chien, S. Y. Lu and C. C. Hu, *Adv. Mater*., 2010, **22**, 347-351.

14 (*a*) S. Chen and S. Qiao, *ACS Nano*, 2013, **7**, 10190-10196; (*b*) R. Chen, H.-Y. Wang, J Miao and H. Yang, *Nano Energy*, 2015, **11**, 333-340.

15 (*a*) G. Q. Zhang and X. W. Lou, *Adv. Mater*., 2013, **25**, 976-979; (*b*) L. Yu, G. Q. Zhang, C. Z. Yuan and X. W. Lou, *Chem. Commun*., 2013, **49**, 137-139; (*c*) R. Ding, L. Qi, M. J. Jia and H. Y. Wang, *J. Appl. Electrochem*., 2013, **43**, 903-910.

16 B. Cui, H. Lin, J.-B. Li, X. Li, J. Yang and J. Tao, *Adv. Funct. Mater*., 2008, **18**, 1440-1447.

17 (*a*) J. Liang, Z. Fan, S. Chen, S. Ding and G. Yang, *Chem. Mater*., 2014, **26**, 4354-4360. (*b*) C. Z. Yuan, L. Yang, L. R. Hou, J. Y. Li, Y. X. Sun, X. G. Zhang, L. F. Shen, X. J. Lu, S. L. Xiong and X. W. Lou, *Adv. Funct. Mater*. 2012, **22**, 2560-2566.

18 (*a*) M. Gong, Y. G. Li, H. L. Wang, Y. Y. Liang, J. Z. Wu, J. G. Zhou, J. Wang, T. Regier, F. Wei and H. J. Dai, *J. Am. Chem. Soc*., 2013, **135**, 8452-8455; (*b*) S. Chen, J. J. Duan, M. Jaroniec and S. Z. Qiao, *Angew. Chem. Int. Ed*., 2013, **52**, 13567-13570; (*c*) Y. Zhang, B. Cui, C. S. Zhao, H. Lin and J. B. Li, *Phys. Chem. Chem. Phys*., 2013, **15**, 7363-7369; (*d*) X. Zou, A. Goswami and T. Asefa, *J. Am. Chem. Soc*., 2013, **135**, 17242-17245.

19 (*a*) F. Song and X. L. Hu, *Nat. Commun*., 2014, **5**, 4477-4486; (*b*) F. Song and X. L. Hu, *J. Am. Chem. Soc*., 2014, **136**, 16481-16484.

20 L. Huang, D. Chen, Y. Ding, S. Feng, Z. L. Wang and M. Liu, *Nano Lett*., 2013, **13**, 3135-3139.

21 (*a*) S. J. Shi and G. H. Zhao, *J. Phys. Chem. C* 2014, **118**, 25939-25946. (*b*) M.-C. Liu, L.-B. Kong, C. Lu, X.-M. Li, Y.-C. Luo and L. Kang, *ACS Appl. Mater. Interfaces,* 2012, **4**, 4631-4636.

22 (*a*) W. F. Wei, W. X. Chen and D. G. Ivey, *Chem. Mater.* 2008**, 20**, 1941-1947; (*b*) S. B. Wang, Y. D. Hou and X. C. Chen, *ACS Appl. Mater. Interfaces,* 2015, 7, 4327-4335; (*c*) S. B. Wang, Z. X. Ding and X. C. Chen, *Chem. Commun*., 2015, **51**, 1517-1519.

23 M. A. Peck and M. A. Langell, *Chem. Mater.* 2012, **24**, 4483-4490.

24 A. B. F. Martinson, S. C. Riha, E. J. Thimsen, W. Elam and M. J. Pellin, *Energy Environ. Sci*., 2013, **6**, 1868-1878.

25 (*a*) A. J. Koza, Z. He, S. Miller and A. J. Switzer, *Chem. Mater.*, 2012, **24**, 3567-3573. (*b*) C. Wu, S. Deng, H. Wang, Y. Sun, J. Liu and H. Yan, *ACS Appl. Mater. Interfaces*, 2014, **6**, 1106-1112.

26 A. J. Bard, *L. R. F. Wiley*: New York **1980**, 1-864.

27 L. An, P. Zhou, J. Yin, H. Liu, F. Chen, H. Liu, Y. Du and P. Xi, *Inorg. Chem*., 2015, **54**, 3281-3289.

28 J. Xie, J. Zhang, S. Li, F. Grote, X. Zhang, H. Zhang, R. Wang, Y. Lei, B. Pan and Y. Xie, *J. Am. Chem. Soc*., 2013, **135**, 17881-17888.

29 L. Wang, C. Lin, D. Huang, F. Zhang, M. Wang and J. Jin, *ACS Appl. Mater. Interfaces*, 2014, **6**, 10172-10180.

30 (*a*) H. W. Park, D. U. Lee, Y. Liu, J. Wu, L. F. Nazar and Z. Chen, *J. Electrochem. Soc*., 2013, **160**, 2244-2250; (*b*) S. Chen, J. Duan, M. Jaroniec and S. Qiao, *Adv. Mater*., 2014, **26**, 2925-2930; (*c*) J. Tian, Q. Liu, A. M. Asiri, K. A. Alamry and X. Sun, *ChemSusChem*, 2014, **7**, 2125-2130.

31 J. Wang, H. Zhang, Y. Qin and X. Zhang, *Angew. Chem. Int. Ed*., 2013, **52**, 5248-5253.

32 (*a*) T. Grewe, X. Deng, C.; Schüth, F.; Tüysüz, H. *Chem. Mater.* **2013**, *25*, 4926-4935. (b) Tüysüz, H.; Hwang, Y. J.; Khan, S. B.; Asiri, A. M.; Yang, P. *Nano Res.* **2013**, *6*, 47-54.

33 (*a*) Wu, J.; Xue, Y.; Yan, X. Weidenthaler, W. Yan, Q. Cheng and Y. Xie, *Nano Res*., 2012, **5**, 521-530; (*b*) A. Schechter, M. Stanevsky, A. Mahammed and Z. Gross, *Inorg. Chem*., 2012, **51**, 22-24.

34 T.-Y. Ma, S. Dai, M. Jaronies and S. Z. Qiao, *J. Am. Chem. Soc*., 2014, **136**, 13925-13931.

35 H. Jin, J. Wang, D. Su, Z. Wei, Z. Pang and Y. Wang, *J. Am. Chem. Soc*., 2015, **137**, 2688-2694.

Nanoscale Accepted Manuscript

36 L. Wu, Q. Li, C. H. Wu, H. Zhu, A. Mendoza-Garcia, B. Shen, J. Guo and S. Sun, *J. Am. Chem. Soc*., 2015, **137**, 7071-7074.
37 M.-R. Gao, X. Cao, Q. Gao, Y.-F. Xu, Y.-R. Zheng, J. Jiang and S.-H. Yu, *ACS Nano*, 2014, **8**, 3970-3978.
38 E. J. Popczun, J. R. McKone, C. G. Read, A. J. Biacchi, A. M. Wiltrout, N. S. Lewis and R. E. Schaak, *J. Am. Chem. Soc*., 2013, **135**, 9267-9270.
39 (*a*) B. E. Conway and B. V. Tilak, *Electrochim. Acta*, 2002, **47**, 3571-3594; (*b*) Y.-F. Xu, M.-R. Gao, Y.-R. Zheng, J. Jiang and S. H. Yu, *Angew. Chem. Int. Ed*., 2013, **52**, 8546-8550; (*c*) N. Pentland, J. O. M. Bockris and E. Sheldon, *J. Electrochem. Soc*., 1957, **104**, 1-82.
40 (*a*) Y. Li, H. Wang, L. Xie, Y. Liang, G. Liang and H. Dai, *J. Am.Chem. Soc*., 2011, **133**, 7296-7299; (*b*) W. Zhou, D. Hou, Y. Sang, S. Yao, J. Zhou, G. Li, L. Li, H. Liu and S. Chen, *J. Mater. Chem. A*., 2014, **2**, 11358-11364; (*c*) J. G. N. Thomas, *Trans. Faraday Soc*., 1961, **57**, 1603-1611.
41 Y. Liang, H. Wang, J. Zhou, Y. Li, J. Wang, T. Regier and H. Dai, *J. Am. Chem. Soc*., 2012, **134**, 3517-3523.
42 J. Tian, Q. Liu, N. Cheng, A. M. Asiri and X. Sun, *Angew. Chem. Int. Ed*., 2014, **53**, 9577-9581.
43 T. F. Jaramillo, K. P. Jørgensen, J. Bonde, J. H. Nielsen, S. Nielsen and I. Chorkendorff, *Science*, 2007, **317**, 100-102.
44 J. Xie, H. Zhang, S. Li, R. Wang, X. Wang, M. Zhou, J. Zhou, X. Zhou and Y. Xie, *Adv. Mater*., 2013, **25**, 5807-5813.
45 J. Liu, Q. Liu, A. M. Asiri and X. Sun, *J. Am. Chem. Soc*., 2014, **136**, 7587-7590.
46 J. Bao, X. Zhang, B. Fan, J. Zhang, M. Zhou, W. Yang, X. Hu, H. Wang, B. Pan and Y. Xie, *Angew. Chem. Int. Ed*., 2015, **54**, 7399-7404.
47 (*a*) X.-F. Lu, D.-J. Wu, R.-Z. Li, Q. Li, S.-H. Ye, Y.-X. Tong and G.-R. Li, *J. Mater. Chem. A,* 2014, **2**, 4706-4713; (*b*) T. Choudhury, S. Saied, J. Sullivan and A. Abbot, *J. Phys. D*, 1989, **22**, 1185-1195.
48 Y. E. Roginskaya, O. Morozova, E. Lubnin, Y. E. Ulitina, G. Lopukhova and S. Trasatti, *Langmuir*, 1997, **13**, 4621-4627.
49 V. Jiménez, A. Fernández, J. Espinós and A. Gonzélez-Elipe, *J. Electron Spectrosc. Relat. Phenom*., 1995, **71**, 61-71.
50 M. Gong, W. Zhou, M.-C. Tsai, J. G. Zhou, M. Y. Guan, M.-C. Lin, B. Zhang, Y. F. Hu, D.-Y. Wang, J. Y, S. J. Pennycook, B.-J. Hwang and H. J. Dai, *Nat. Commun*., 2014, 1-6.
51 Z. Li, A. L. K. Lui, K. H. Lam, L. Xi and Y. M. Lam, *Inorg. Chem*., 2014, **53**, 10874-10880.
52 J. Tian, Q. Liu, Y. Liang, Z. Xing, A. M. Asiri and X. Sun, *ACS Appl. Mater. Interfaces*, 2014, **6**, 20579-20584.

Nanoscale Accepted Manuscript

This journal is © The Royal Society of Chemistry 20xx